Neoplasia 62 (2025) 101150

Contents lists available at ScienceDirect

Neoplasia

journal homepage: www.elsevier.com/locate/neo

Original Research

HRP2 regulating MICU1-mediated Ca^{2+} overload to dictate chemoresistance of multiple myeloma

Qian Li [a,1], Ziyi Peng [b,1], Li Lin [c], Zhiying Zhang [c], Jing Ma [c], Lin Chen [c], Su Liu [c], Shuang Gao [c], Linchuang Jia [b], Jingjing Wang [d], Zeng Cao [a], Xingli Zhao [e,*], Zhiqiang Liu [d,**], Yafei Wang [a,***]

[a] Department of Hematology, Tianjin Medical University Cancer Institute and Hospital; National Clinical Research Center of Cancer; Tianjin Key Laboratory of Cancer Prevention and Therapy; Tianjin's Clinical Research Center of Cancer, Tianjin, 300060 China
[b] Department of Physiology and Pathophysiology, School of Basic Medical Science, Tianjin Medical University, Heping, Tianjin, 300070 China
[c] Department of Blood and Marrow Transplantation, Tianjin Cancer Hospital Airport Hospital, Tianjin 300308, China
[d] Shandong Provincial Key Laboratory of Precision Oncology, Shandong Cancer Hospital and Institute, Shandong First Medical University and Shandong Academy of Medical Sciences, Jinan, 250117, China
[e] Department of Hematology, Oncology Center, Tianjin Union Medical Center, Hongqiao, Tianjin, 300122, China

ARTICLE INFO

Keywords:
Multiple myeloma
Chemoresistance
HRP2
MICU1
Ca^{2+} overload

ABSTRACT

Despite the efficacy of bortezomib (BTZ)-based chemotherapy in treating multiple myeloma (MM) patients, chemoresistance occurs frequently over time, particularly in individuals exhibiting an initial positive response to BTZ therapy. In this study, we established BTZ-resistant MM cells and identified that suppressed expression of the hepatoma-derived growth factor (HDGF)-related protein-2 (HRP2) was a key determinant of chemoresistance in MM cells. Manipulating HRP2 expression remodeled the chemosensitivity of MM cells in vitro and in vivo. Clinically, lower expression of HRP2 predicted a shorter survival rate in MM patients receiving BTZ-based regimens. Mechanistically, HRP2 depletion resulted in elevated acetylation modifications of histone 3 at lysine 27 (H3K27Ac), and enhanced chromatin accessibility as well as transcriptional elongation of mitochondrial calcium uptake 1(MICU1) gene, thus promoting the expression of MICU1 gene and alleviating calcium (Ca^{2+}) overload and excessive reactive oxygen species (ROS) induced mitochondria damage and apoptosis in MM cells. Thereby, MICU1 suppression improved BTZ sensitivity in vitro and relieved tumor burden in a mouse model of MM. Similarly, elevated MICU1 expression was observed in the $B220^{+}CD19^{+}$ B cells from HRP2-knockout mice and significantly correlated with poor prognosis in the clinic. Thus, our study elucidates the previously unrecognized epigenetic role of HRP2 in regulating calcium homeostasis of MM cells, providing new theoretical insights into the mechanisms underlying the development of drug resistance in multiple myeloma.

Introduction

Multiple myeloma (MM) is the second most common hematologic malignancy, distinguished by uncontrolled proliferation of terminally differentiated plasma cells and extensive infiltration of monoclonal immunoglobulin protein (M protein) in the bone marrow [1,2]. Despite the significant advancements in improving the response rates of MM patients through the introduction of novel agents like proteasome inhibitors, immunomodulatory drugs, monoclonal antibodies, and CAR T cell therapies [3,4], MM remains an elusive adversary with no definitive cure. Despite progress, a significant proportion of patients inevitably experience relapse, thereby limiting the options for new treatment approaches [5,6]. Therefore, it is critical to elucidate the mechanisms of drug resistance to develop novel strategies for better outcomes.

HRP2 belongs to the HDGF-related protein family [7], sharing a common characteristic of binding to DNA through the HATH/PWWP

* Corresponding author at: Department of Hematology, Oncology Center, Tianjin Union Medical Center, Hongqiao, Tianjin, 300122, China.
** Corresponding author at: Shandong Cancer Hospital and Institute, Shandong First Medical University and Shandong Academy of Medical Sciences, Jinan, 250117, China.
*** Corresponding author at: Department of Hematology, Tianjin Medical University Cancer Institute and Hospital, Tianjin, 300060, China.
E-mail addresses: insectzhao@163.com (X. Zhao), zqliu@sdfmu.edu.cn (Z. Liu), yfwang@tmu.edu.cn (Y. Wang).
[1] These authors contribute equally to this work.

https://doi.org/10.1016/j.neo.2025.101150
Received 24 September 2024; Accepted 27 February 2025

domain located at the N-terminus [8]. Recent research has implicated HRP2 in the progression of cancer [9,10]. In patients with t(4;14) multiple myeloma (MM), overexpression of NSD2 leads to high levels of H 3K36 dimethylation (H 3K36me2) [11]. HRP2 functions as reader of histone H 3K36 methylation [12], and the HRP2-MINA complex mediates chromatin modifications and transcriptome alterations in MM, indicating that HRP2 may play a pivotal role in regulating chemosensitivity and apoptosis in this context [13]. However, the mechanism by which HRP2 regulates downstream signaling pathways in MM remains unclear.

MICU1 serves as a crucial and essential regulator of mitochondrial Ca^{2+} uptake [14], functioning as a component of the mitochondrial Ca^{2+} uniporter channel complex (mtCU). This complex comprises of the mitochondrial calcium uniporter protein (MCU), the MCU dominant-negative β-subunit (MCUb) and essential MCU regulator (EMRE), namely MICU1 and MICU2. These entities collaboratively prevent the occurrence of mitochondrial Ca^{2+} overload [15,16]. The mitochondrial membrane potential (MMP) facilitates Ca^{2+} transport through the MCU, with MICU1 orchestrating the regulation of MCU to impart Ca^{2+} sensitivity [17,18]. In the absence of this regulatory complex, an influx of Ca^{2+} into mitochondria occurs, leading to excessive mitochondrial Ca^{2+} overload and subsequent mitochondria damage. This overload results in an increased production of reactive oxygen species (ROS) generation and heightened sensitivity to apoptotic stress [15,19]. Recent findings have indicated high MICU1 expression in chemo-resistant high grade serous ovarian cancer (HGSOC) tissues where MICU1 overexpression correlates with poor overall survival (OS) in ovarian cancer patients [20]. However, the specific role of MICU1 in provoking chemoresistance in MM cells induced by proteasome inhibitor remains unclear. Elucidating these intricacies will contribute to a deeper understanding of the molecular pathways involved in mitochondrial function and drug response in MM.

Material and methods

Cell culture

MM cell lines MM.1S and LP-1 were purchased from the National Infrastructure of Cell Line Resource (Beijing, China). Authentications were conducted using short tandem repeat (STR) analysis (Biowing Biotech) and mycoplasma-free were assured using Universal Mycoplasma Detection Kit (ATCC). Culture of MM cells and the tool HEK293T cells have been detailed in our previous study [21]. To develop BTZ-resistant MM cells, parental drug-naive cells were subjected to a gradual escalation of BTZ exposure, starting at 0.5 nM and doubling every monthly for 6 months. The acquisition of BTZ-resistant phenotype was monitored and validated by assessing the IC_{50} of BTZ using the MTS assay.

Transfection, virus package and infection

Transient transfections were performed on HEK293T cells using polyethyleneimine (PEI) (Polysciences) in the OPTI-MEM medium (Life Technologies) with a DNA: PEI ratio ranging from 1:4 to 1:6. Viral particles were produced by transfecting HEK293T cells in a 10 cm dish with 4 μg pMD2.G and 6 μg psPAX2 packaging plasmids (Addgene), together with 8 μg lentiviral expressing vectors encoding target genes, including pITA-HRP2, pITA-MICU1, pLKO.1 vector encoding shRNAs targeting HRP2 and MICU1 genes. The supernatant carrying the viral particles was harvested at 36 h and 60 h after transfection and concentrated to 100 × volume by Poly (ethylene glycol) 8000 (Sigma-Aldrich).

For viral infection, 1×10^6 MM cells were seeded in 1 ml fresh complete media for 6 h, after which 50 μl of viral concentration and 8 μg/ml polybrene were added, and cells were spun at 1800 rpm for 45 min at 20°C. 12 h after infection, the medium was replaced, and cells were cultured for an additional 48 h for subsequent utilization.

RNA-sequencing

Cells were treated total RNA was extracted from two biological replicates. RNA quality was assessed using a 2100 Expert Bioanalyzer (Agilent) and then sent for library preparation and sequencing using the Illumina Hiseq2000 platform of Majorbio Biotech (Shanghai, China). The data were analyzed on the free online Majorbio I-Sanger Cloud Platform UENCING.

Real-time PCR

Detailed procedures for real-time PCR can be found in our previously published report [21]. The primer sequences used in qPCR were listed as follows. HRP2 (Forward: CGTGAAGAGGTGCCTGAATG; Reverse: ACTTCTGCTGCCTTCTCCAT); MICU1 (Forward: GAGGCAGCTCAAGAAGCACT; Reverse: CAAACACCACATCACACACG); GAPDH (Forward: AATGGGCAGCCGTTAGGAAA; Reverse: GCCCAATACGACCAAATCAGAG). The relative expression levels of target mRNA in samples were determined by normalization to the control housekeeping gene GAPDH using the $2^{-\Delta\Delta Ct}$ method.

Western blotting

Cell lysis was carried out by using RIPA buffer supplemented with protease inhibitors (Roche), and nuclear and cytoplasmic protein extraction was performed with NE-PER Nuclear and Cytoplasmic Extraction Kit (Thermo Fisher Scientific). 100 μg of total lysate was loaded onto the SDS-PAGE gel, and the protein were transferred onto the nitrocellulose membranes (Pall Corporation, Washington, NY, USA). After membrane blocking, the membranes were incubated with the indicated antibody at 4°C overnight. Then the membrane was washed and incubated with horseradish peroxidase-conjugated secondary antibodies and finally visualized using an enhanced chemiluminescence system (Millipore). The antibodies used in the present study included HRP2 (Proteintech), MICU1 (Cell Signaling Technology) and β-actin (Abclonal).

Flow cytometry for apoptosis

Apoptotic cells were measured using an Annexin V-FITC Apoptosis Detection Kit (Sigma-Aldrich) following to the previous protocol [22]. A total of 1×10^5 cells were stained with 5 μl Annexin V-FITC and 1 μl of propidium iodide and then analyzed by a FACS Calibur instrument. The data of flow cytometry were analyzed using FlowJo v10.

Calcium measurement

Mitochondrial Ca^{2+} measurements were carried out using Rhod-2 AM(Invitrogen). To label mitochondria, cells were treated with MitoTracker® Green (Cell Signaling Technology). Briefly, MM cells were transfected as described earlier. 48 h after transfection, live MM cells were incubated with MitoTracker® Green and Rhod-2 AM at 37°C for 30 min. Following three washes with 1 × PBS, imaging was performed using a fluorescence microscope (model IX71; Olympus).

Measurement of mitochondrial ROS levels

To quantify superoxide generation in the MM cells, FACS analysis was conducted utilizing MitoSOX (Invitrogen). As a positive control, 1 mM respiratory inhibitor rotenone was used, known to elevate superoxide levels by inhibiting respiratory complex I [23]. Briefly, MM cells were treated with 5 μM MitoSOX™ reagent working solution and incubated cells for 10 min at 37°C, while protected from light. After three washes with 1 × PBS, the cells were analyzed on a BD FACS flow

cytometer.

Mice and ethic approvals

The NOD-*scid* IL2Rgamma^{null} (NSG) mice and HRP2-KO mice were obtained from Cyagen Bioscience (Suzhou). Mice age 6-8 week were used in this study after matching gender, and the usage of mice in these studies was approved by the Tianjin Medical University Committee of Animal Research and Ethics, and all protocols followed the Guidelines for Ethical Conduct in the Care and Use of Nonhuman Animals in Research.

ChIP-qPCR and reanalysis of ATAC-seq assay

A detailed protocol for the ChIP assay has been stated in our previous studies [24]. For ChIP-qPCR assay, chromatin immunoprecipitation was elicited by antibodies against H 3K36Ac, or p-RNA pol II CTD (Ser2, Ser5, Ser7), and the pulldown chromatins were detected by real-time PCR with primers specific for the promoter regions of *MICU1* gene.

For a detailed protocol for the ATAC-seq please refer to our previous publication [25]. Re-analysis of the ATAC-seq data for the chromatin accessibility of MICU1 gene was done by the Integrative Genomics Viewer (Broad Institute, UC San Diego).

Mouse models of MM

4-6 weeks old female NSG mice were used to establish the xenograft and intra-bone models of MM as previously reported ($n = 12$) [26]. After 3 weeks when tumor sizes reached palpable dimensions of ~5 mm diameter, BTZ (0.5 mg/kg) was administrated intraperitoneally three times per week. MicroCT imaging of mouse femurs was performed using a Skyscan 1172 microtomograph (BrukermicroCT). After segmentation, the 3D models were constructed from the stack of 2D images using a surface-rendering program (Ant, release 2.0.5, Skyscan). 3D measurements were obtained with the CtAn software (release 2.5, Skyscan). Trabecular bone analysis was specifically performed on the femur body. With the calculation of the following 3D parameters: trabecular volume (BV/TV, in %), trabecular thickness (Tb. Th, in μm), trabecular separation (Tb. Sp. in μm) and trabecular number (Tb. N, in 1/mm).

Statistical analysis

Data were shown as mean ± SD form at least three independent experiments. Differences between groups were determined using paired two-sided Student's t-test or two-way ANOVA. Pearson correlation test was used to determine the correlations between gene expressions. Survival analysis and a log-rank test were conducted via GraphPad Prism 5.0. A P value <0.05 was considered statistically significant when compared to the controls, respectively.

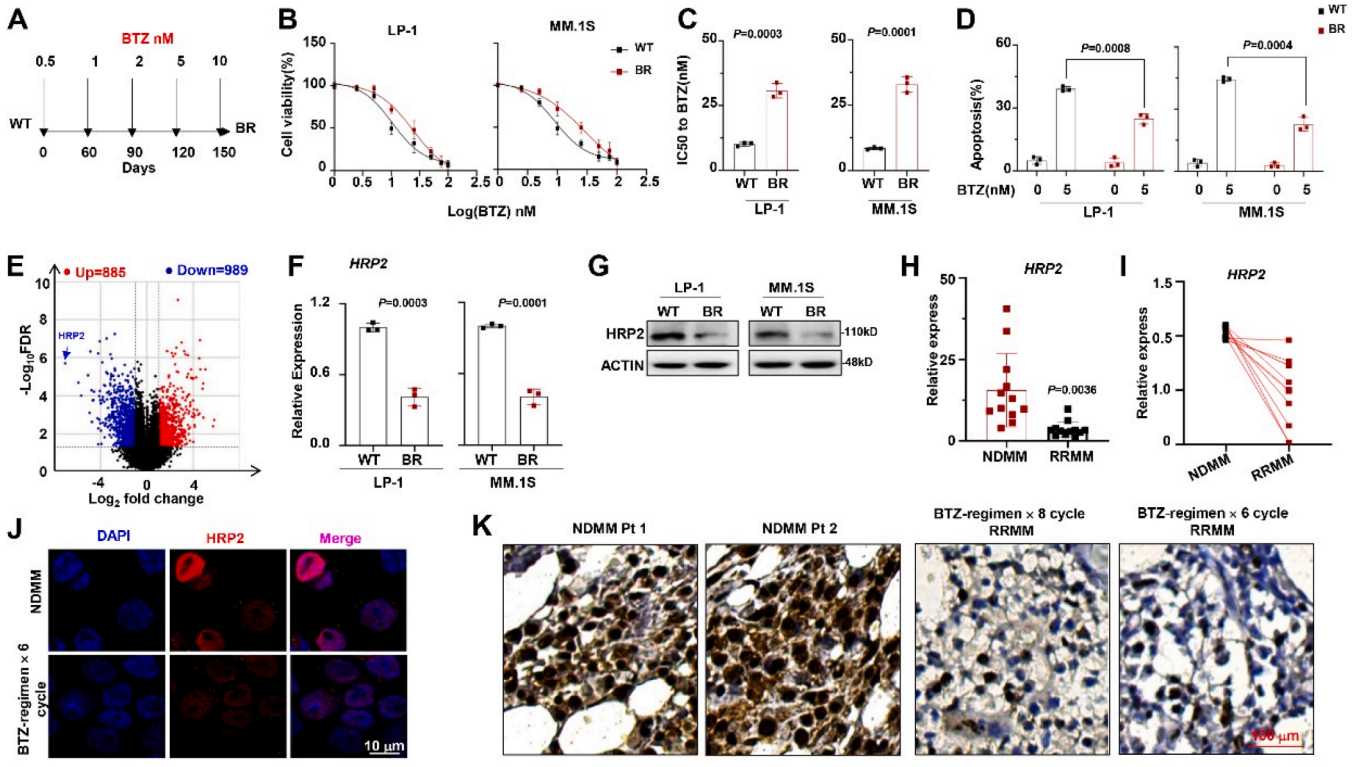

Fig. 1. HRP2 is associated with bortezomib treatment sensitivity in MM.
(A) Diagram of induction of BTZ resistance in human MM cell lines. Cells were exposed to increasing concentrations of BTZ for three months. **(B)** Alteration of IC_{50} to BTZ treatment in the wild type (WT) and BTZ-resistant (BR) LP-1 and MM.1 s cells. **(C)** Comparison of the IC_{50} values between WT and BR cells ($n = 3$). **(D)** Flow cytometry analysis depicting apoptosis of WT and BR cells after BTZ treatment. ($n = 6$) **(E)** Volcano plot of differentially expressed genes analyzed from RNA-sequencing in MM.1S BR and WT cells. Blue represents downregulated genes; red represents upregulated genes; and gray indicates statistically non-significance genes. **(F)** HRP2 mRNA levels and **(G)** corresponding protein expression in BR LP-1 and MM.1 s cells in comparison to WT controls. **(H)** *HPR2* levels in patients with newly diagnosed multiple myeloma (NDMM) and relapsed or refractory multiple myeloma (RRMM) ($n = 12$). **(I)** Changes in *HPR2* levels in the same patients during MM progression ($n = 10$). P values were determined by Pearson Coefficient and Log-ranks test. Two-sided P values were determined by Student's t-test. Data are presented as mean ± SD. **(J)** Immunofluorescence analysis for HRP2 (red) in NDMM and BTZ-regimen × 6 cycle RRMM patient. Nuclei were stained with DAPI (blue). Scale bar: 10 μm. **(K)** Immunohistochemical images of bone marrow biopsies from NDMM or RRMM MM patients. Scale bar: 100 μm.

Result

HRP2 is downregulated in the BTZ-resistant MM cells

To investigate the characteristics of BTZ-induced resistance in MM, we established BTZ-resistant (BR) LP-1 and MM.1S cells that can survive treatment with 10 nM BTZ (Fig. 1**A**). After induction, we observed a significant increase in the IC_{50} for BTZ (Fig. 1**B**, 1**C**), accompanied by a markedly reduced apoptosis rate of the BR-MM cells (Fig. 1**D**). To identify differentially expressed genes (DEGs) associated with BTZ-resistance, we utilized bulk RNA-sequencing analysis to screen DEGs of MM.1S BR-cells. The analysis revealed that 885 genes were upregulated, while 989 genes were downregulated in the BR cells compared to the WT cells. Among these genes, HRP2 prominently emerged as one of the top downregulated genes (Fig. 1**E**). Subsequentially, we evaluated the expression of HRP2 in the BR and WT MM cells, observing reduced levels of both protein and mRNA in the BR cells (Fig. 1**F**, 1**G**). Clinically, we examined HRP2 levels in newly diagnosed MM (NDMM) patients and those with relapsed or refractory MM (RRMM) after 6 cycles of treatment with BTZ-based regimens. HRP2 levels were observed to significantly decrease during disease progression compared to the levels at the time of initial diagnosis (Fig. 1**H**). Furthermore, when comparing the bone marrow samples of 10 MM patients, we observed a significant decrease in HRP2 expression at mRNA and protein levels (Fig. 1**I**-1**K**). These results indicate that low HRP2 expression is associated with BTZ resistance in MM cells and correlates with poor outcomes in the clinic.

Overexpression of HRP2 enhances sensitivity to BTZ treatment in vitro and in vivo

Given the association between HRP2 expression and MM chemoresistance, we investigated whether modulation of HRP2 expression affects MM drug resistance. We suppressed HRP2 expression using short-hairpin RNA (shRNA) in LP-1 and MM.1S MM cells (Fig. 2**A**). As a result, the reduction in HRP2 expression significantly increased the IC_{50} values for BTZ (Fig. 2**B**, 2**C**), and meaningfully reduced the apoptosis ratio of MM cells treated with BTZ in both LP-1 and MM.1S cells (Fig. 2**D**). On the contrary, ectopic expression of HRP2 either in wild type or in the BR LP-1 and MM.1 s cells (Fig. 2**E, S 1A**), both remarkably augmented the IC_{50} value (Fig. 2**F,** 2**G, S 1B-1C**) while also significantly impaired the anti-apoptotic capacity of BTZ (Fig. 2**H, S1D**).

To further evaluate the effects of HRP2 on MM tumor growth and BTZ sensitivity in vivo, we established HRP2-OE and the control MM-derived xenograft mouse and intra-bone models of MM [13]. We observed that mice bearing HRP2-OE MM cells had a considerably reduced tumor growth and improved survival rate than the vector controls (Fig. 2**I,** 2**J**). Additionally, mice with intra-bone bearing HRP2-OE MM cells exhibited a marked reduction in bone lesion, indicated by femoral trabecular microstructure (Fig. 2**K**, 2**L**), as well as quantification of bone volume density (BV/TV), trabecular numbers (Tb. N), trabecular thickness (Tb. Th), and trabecular separation (Tb. Sp) **(Fig. S 2A-2D)**. These data collectively demonstrate that HRP2 is a key regulator of sensitivity to BTZ in MM cells.

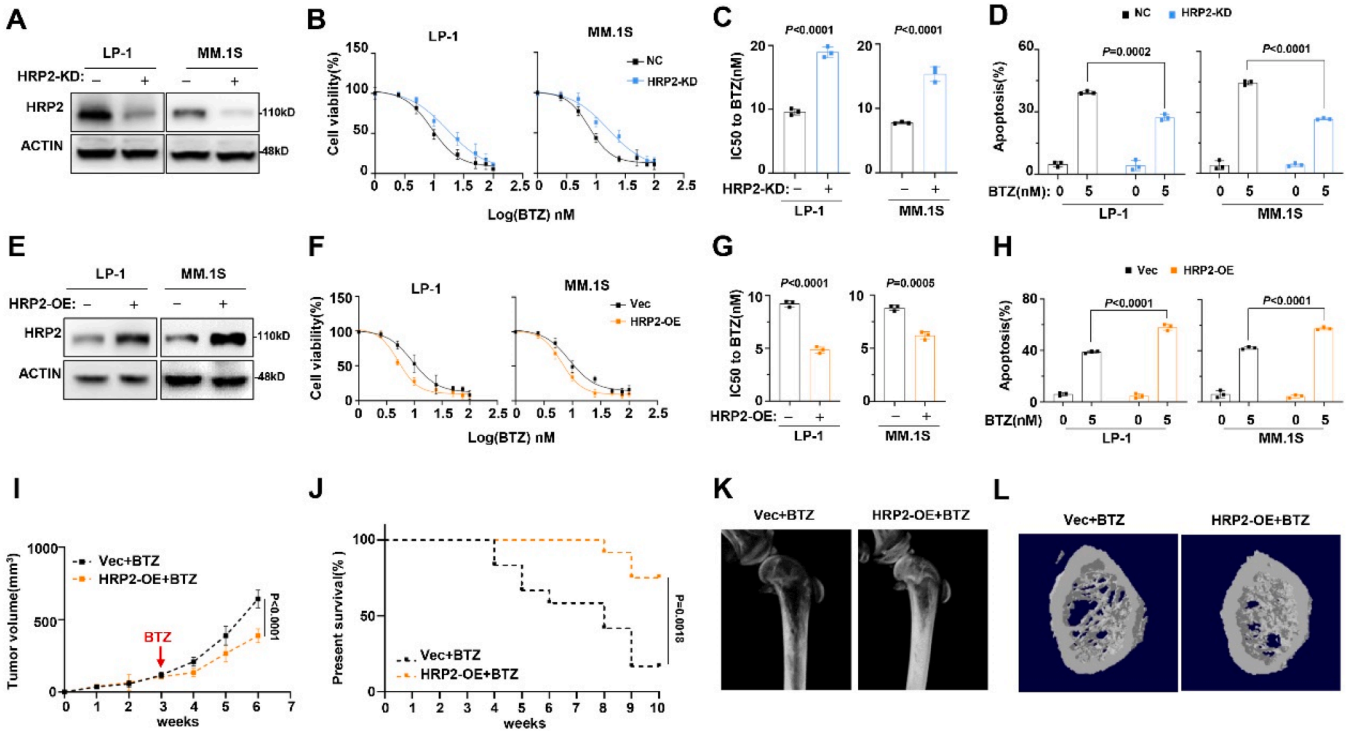

Fig. 2. Overexpressing HRP2 enhances sensitivity to BTZ treatment *in vitro* and *in vivo*.
(A) Western blotting shows the knockdown effects in LP-1 and MM.1 s cells infected with lentivirus carrying shRNA targeting HRP2 gene compared to the non-target control (NC). **(B)** Alteration in the IC_{50} for BTZ treatment in the NC and HRP2 knockdown (HRP2-KD) cells and **(C)** Comparison of the IC_{50} values in NC and HRP2-KD cells ($n = 3$). **(D)** Frequency of apoptosis cells after BTZ treatment. **(E)** Western blot shows the ectopic expression of HRP2 in LP-1 and MM.1 s cells infected with lentivirus carrying the HRP2-overexpression plasmids (HRP2-OE) compared to the vector control (Vec). **(F)** Alteration in the IC_{50} for BTZ treatment in the Vec and HRP2-OE cells and **(G)** comparison of the IC_{50} values in Vec and HRP2-OE cells. ($n = 3$). **(H)** Frequency of apoptosis cells after BTZ treatment. Two-sided P-values were determined by two-way ANOVA test, and data are presented as mean ± SD. **(I)** Growth curve of BTZ treated bearing tumors in mice, derived from MM.1S Vec and HRP2-OE cells ($n = 6$). **(J)** Kaplan-Meier curves showing the survival of mice with BTZ-treated bearing tumors, derived from MM.1S Vec and HRP2-OE cells ($n = 12$). Two-sided *P*-values were analyzed using log-rank test; data are presented as mean ± SD. **(K)** Representative microCT reconstructions of mouse femurs bearing tumors derived from MM.1S Vec and HRP2-OE cells and treated with BTZ ($n = 6$). **(L)** 3D reconstructions of bone trabecula in metaphyseal regions ($n = 6$). Two-sided P-values were determined by two-way ANOVA test, and data are presented as mean ± SD.

HRP2 negatively regulates MICU1 expression

Based on the above corroboratory evidence, we evaluated the impact of HRP2 depletion on transcriptome. In the bulk RNA-seq analysis of the HRP2-KD cells, we observed expression of MICU1 was remarkably elevated among 186 upregulated genes (Fig. 3**A**, 3**B**), and the gene set enrichment analysis identified that the up-regulated genes were associated with enrichment of mitochondrial function-related pathway (Fig. 3**C**). Our result also confirmed that mRNA level of MICU1 was upregulated with HRP2 suppression (Fig. 3**D**), but not other members of the MCU complex (**Fig. S 3A, 3B**), suggesting a transcriptional regulation on MICU1. Thus, we explored the mechanism by which HRP2 regulates MICU1 expression in MM cells. We examined the most common histone modification marks in LP-1 and MM.1S cells, and found that acetylation at lysine 27 on histone 3 (H3K27ac) was substantially increased upon HRP2 depletion (Fig. 3**E**). To clarify whether H3K27ac abundance negatively correlates with MICU1 transcription, we performed ChIP-seq in LP-1 cells, and found a considerable augmentation of H3K27ac enrichment upon HRP2 depletion on MICU1 promoter (Fig. 3**F**), consequently led to a marked elevation of phosphorylation at serine 5 at RNA Pol II around TSS of MICU1 gene (Fig. 3**G**), which is reported as a marker of initiation during transcription cycle [27]. Notably, HRP2 depletion also resulted in the ampliative chromatin accessibility around MICU1 promoters (Fig. 3**H**), which is similar to what was observed in CD138$^+$ plasma cells from a RRMM patient after receiving 6 cycles of BTZ-based regimen (Fig. 3**I**).

To confirm the regulation of HRP2 on MICU1 in vivo, we constructed a genetically HRP2 knockout mice. As expected, when HRP2 was genetically depleted (Fig. 3**J**), we observed remarkable elevated MICU1 protein and universal augmented H3K27ac levels in the CD220$^+$CD19$^+$ B cells from HRP2-KO mice (Fig. 3**K**), along with enrichment of H3K27ac and RNA Pol II p-Ser 5 around TSS of MICU1 gene (Fig. 3**L**, 3**M**). Collectively, these findings indicate that HRP2 negatively regulates both H3K27ac modification and the transcription of MICU1 genes in MM cells.

MICU1 maintains mitochondrial Ca^{2+} homeostasis to trigger chemoresistance in MM cells

Continuing our investigation into whether MICU1 mediates chemoresistance in MM cells. When MICU1 expression was decimated in LP-1 and MM.1S MM cells (Fig. 4**A**), the IC_{50} values for BTZ was noticeably inhibited (Fig. 4**B**, 4**C**), and the apoptotic percentage of MM cells were all meaningfully augmented (Fig. 4**D**). We evaluated the expression of MICU1 in the BR MM cells, and we found both protein and mRNA levels were elevated compared to the WT MM cells (Fig. 4**E**, 4**F**). Further, when MICU1 expression was decimated in the BR-MM cells (shRNA#2) (Fig. 4**G**), the sensitivity to BTZ treatment was substantially rescued, as evidenced by notably repressed IC50 value and augmented apoptosis ratios (Fig. 4**H-J**). Importantly, MICU1 expression was markedly higher in the RRMM patients than NDMM patients (Fig. 4**K**), and the expression was negatively correlated with HRP2 level in CD138$^+$ plasma cells isolated from RRMM patients (Fig. 4**L**). Additionally, higher MICU1 expression predicted a poorer overall survival rate in an independent

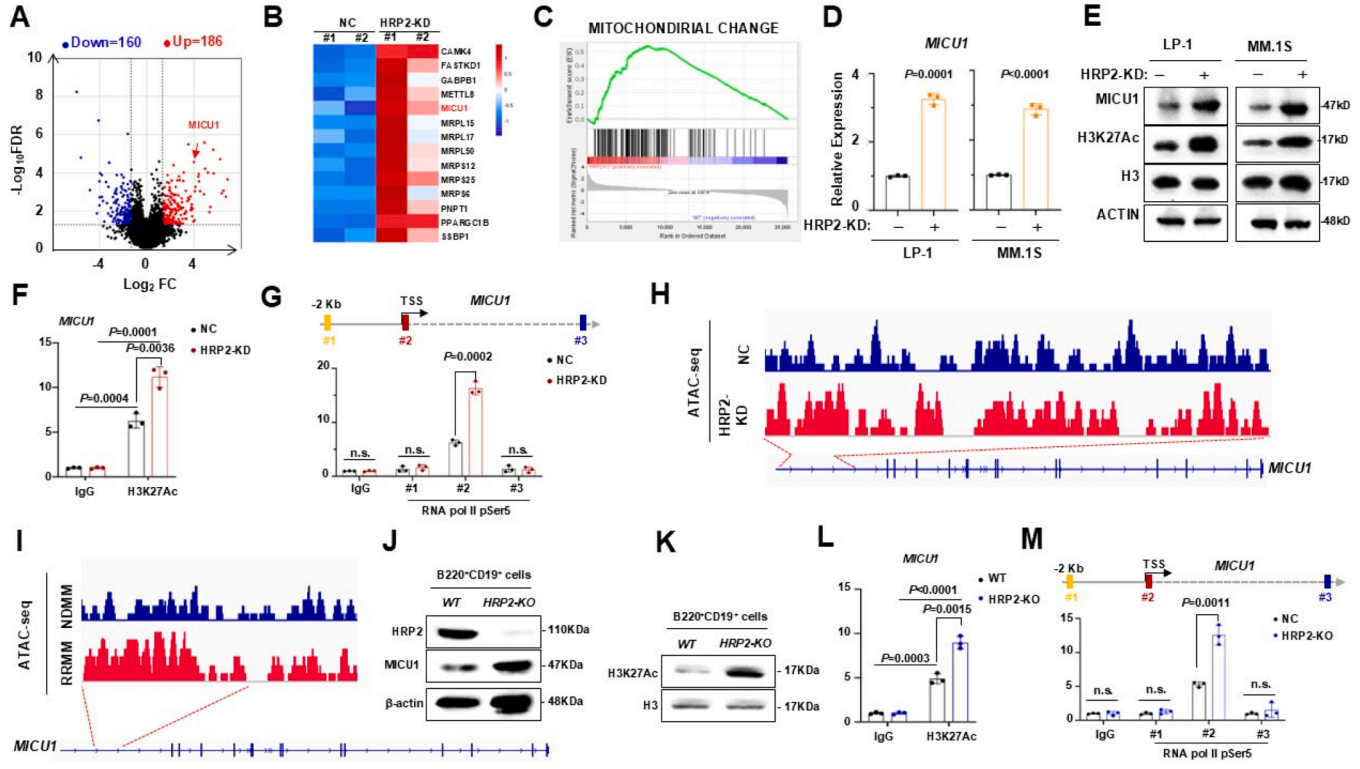

Fig. 3. HRP2 negatively regulates expression of MICU1.
(A) Volcano plot of differentially expressed genes analyzed from RNA-sequencing in HRP2-KD and non-target control (NC) MM.1S cells. Blue denotes downregulated genes; red indicates upregulated genes; and gray represents statistically non-significance genes. **(B)** The gene set enrichment analysis (GSEA) showing up- and down-regulated genes by RNA-sequencing. **(C)** Heat map depicting significantly upregulated genes in HRP2-KD MM cells **(D)** MICU1 mRNA expression in HRP2-OE MM cells compared with the vector control ($n = 3$) **(E)** MICU1 and H3K27Ac protein expression in HRP2-OE MM cells compared with the vector control. **(F)** ChIP-qPCR of H3K27Ac at the MICU1 gene loci in NC and HRP2-KD MM cells ($n = 3$). **(G)** ChIP-qPCR profile for MICU1 genes enriched by RNA Pol II p-Ser5 in NC and HRP2-KD MM cells ($n = 3$). **(H)** Gene tracks showing representative ATAC-Seq profiles at MICU1 gene loci in NC and HRP2-KD MM cells, and **(I)** CD138$^+$ cells from NDMM and RRMM patients. **(J)** The MICU1 and HRP2 protein levels in WT and HRP2-KO mice B cells. **(K)** The H3K27Ac levels in WT and HRP2-KO mice B cells. **(F)** ChIP-qPCR of H3K27Ac at the MICU1 gene loci in WT and HRP2-KO mice B cells ($n = 3$). **(G)** ChIP-qPCR profile for MICU1 genes enriched by RNA Pol II p-Ser5 in WT and HRP2-KO mice B cells. Two-sided P value was determined by Student's t-test. data are presented as mean ± SD.

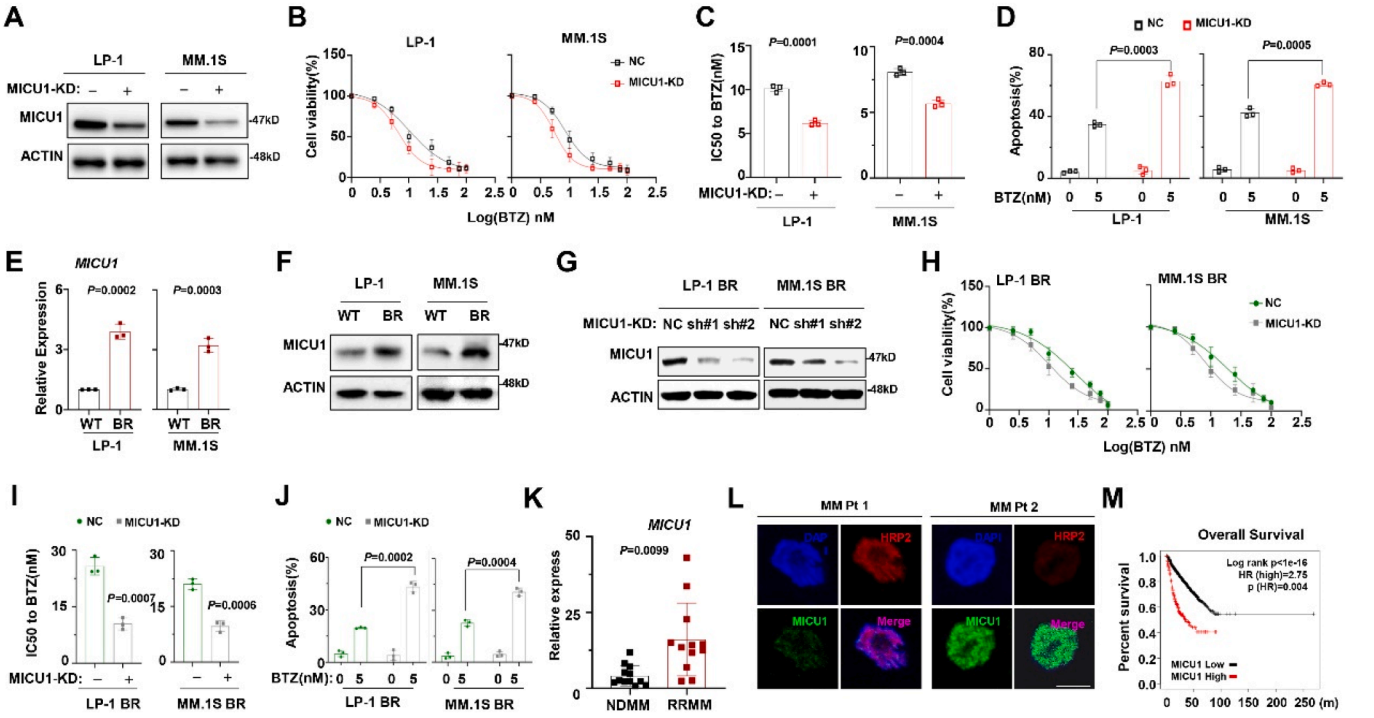

Fig. 4. MICU1 plays critical role in regulating chemosensitivity to BTZ in MM cells.
(A) Western blotting shows the knockdown effects in LP-1 and MM.1 s cells infected with lentivirus carrying shRNA targeting MICU1 gene compared to the non-target control (NC). **(B)** Alteration of IC_{50} to BTZ treatment in the NC and MICU1 knockdown (MICU1-KD) cells and **(C)** comparison of the IC_{50} values in NC and MICU1-KD cells ($n = 3$). **(D)** Frequency of apoptosis cells after BTZ treatment. **(E)** MICU1 mRNA and **(F)** protein expression in BR and WT MM cells ($n = 3$). **(G)** Representative Western blotting ($n = 3$) shows the knockdown effects in LP-1 and MM.1 s BR cells infected with lentivirus carrying shRNAs targeting two different coding sequencing of MICU1 gene (shRNA1, 2) compared to the NC. **(H)** Alteration of IC_{50} to BTZ treatment in the NC and MICU1-KD BR MM cells and **(I)** comparison of the IC_{50} values in NC and MICU1-KD BR MM cells ($n = 3$). **(J)** Frequency of apoptosis cells after BTZ treatment in NC and MICU1-KD BR MM cells. **(K)** *MICU1* level in patients with newly diagnosed multiple myeloma (NDMM) and relapsed or refractory multiple myeloma (RRMM) ($n = 12$). **(L)** Immunofluorescence analysis for HRP2 (red) and MICU1 (green) in MM patients. Nuclei were stained with DAPI (blue). Scale bar: 5 μm. **(M)** Correlation of *MICU1* mRNA expression with Overall Survival (OS) in MM patients. Two-sided P value was determined by Student's t-test. data are presented as mean ± SD.

MM cohort (Fig. 4**M**). These findings suggest that aberrant expression of MICU1 is closely correlated with the adverse prognosis of MM.

Loss of MICU1 exacerbates Ca^{2+} overload and induces stress in mitochondria

Mitochondrial Ca^{2+} uptake, an essential role in aerobic metabolism, is primarily regulated by MICU1 via the calcium uniporter, ensuring calcium homeostasis in mitochondria. Recent studies have shown that loss of MICU1 leads to oxidative stress [19,28,29]. To investigate the MICU1's contribution to MM cell responses to BTZ by modulating mitochondrial Ca^{2+}mitochondria, we utilized MitoTracker and Rhod-2 AM probes targeting mitochondria and mitochondrial $[Ca^{2+}]_m$ in MM cells. The basal $[Ca^{2+}]_m$ was elevated over 2-fold in the MICU1-KD cells as compared to the NC cells (Fig. 5**A**, 5**B**). To complement the findings of Rhod-2 AM indication, we treated the MICU1-KD and parental MM cells with Rhod-2 AM and BTZ in sequence. The results corroborated that MICU1-KD MM cells exhibited an increase in mitochondrial Ca^{2+} uptake after BTZ treatment (Fig. 5**C**). Given that enhanced Ca^{2+} load resulted in mitochondrial oxidative stress [30], we measured superoxide levels using MitoSOX, and the analysis showed a notable increase in the MitoSOX fluorescence intensity in the MICU1-KD MM cells compared to the control (Fig. 5D, Blue represents rotenone, an inhibitor for mitochondrial electron transport chain complex I,serving as a positive control). The quantification of the FACS revealed a >7-fold increase MICU1-KD MM cells (Fig. 5**E**), suggesting a rise in the levels of mitochondrial superoxide. Under the condition that mitochondrial ROS was eradicated by MitoTempo, BTZ treatment failed to induce a significant augmentation in apoptosis rate of MICU1-KD MM cells (Fig. 5**F**). Intriguingly, when HRP2 was forcedly overexpressed, mitochondrial Ca^{2+} uptake was markedly expanded due to BTZ treatment (Fig. 5**G**), HRP2-OE cells exhibited higher mitochondrial superoxide levels compared to Vec MM cells (Fig. 5**H**). In the HRP2 highly expressed MM cells, treatment with BTZ led to radical ROS production (Fig. 5**I**, 5**J**). To assure that the ROS production was triggered by HRP2-MICU1 axis, we suppressed HRP2 expression in the MICU1-KD MM.1S cells, which resulted in the rescue of MICU1 expression (Fig. 5**K**), and observed that treatment of BTZ failed to irritate Ca^{2+} and superoxide load in mitochondria (Fig. 5**L**, 5**M**), and ROS production under stimulation of BTZ less prominent (Fig. 5**N**, 5**O**). These data collectively suggest that MICU1 attributes to the mitochondrial homeostasis of $[Ca^{2+}]_m$ in MM cells, especially under the pressure of BTZ treatment.

Targeting MICU1 sensitizes MM cells to BTZ treatment in vivo

Our findings have indicated a critical role of HRP2-MICU1 axis in modulating Ca2+ homeostasis and chemoresistance of MM cells. To elucidate the significance of targeting the HRP2-MICU1 axis in overcoming BTZ-resistance in MM, we stablished two mouse models of MM by subcutaneously or intra-femur injecting MICU1-KD and control MM cells into NSG mice, respectively (Fig. 6**A**). After three weeks, mice were treated with intraperitoneal injections of 0.5 mg/kg BTZ once the established tumor volume reached approximately 500mm^3. Notably, the tumor growth was significantly suppressed in mice bearing MICU1-KD MM cells group compared to the control group (Fig. 6**B**). Moreover, mice bearing MICU1-KD MM cells had significantly improved overall survival rate (Fig. 6**C**). Similarly, MICU1-KD MM cells growing in the bone marrow microenvironment of mice exhibited an obvious

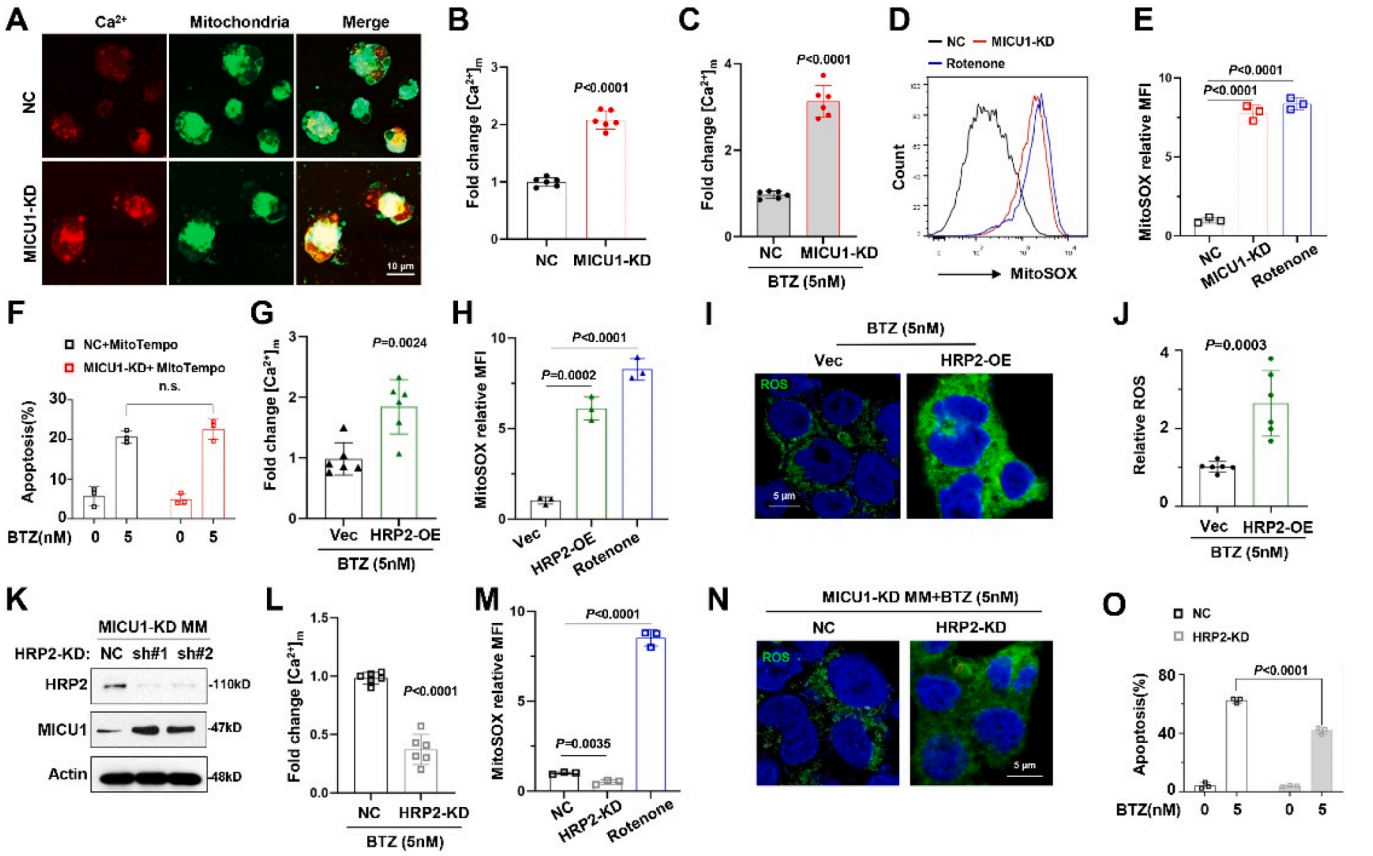

Fig. 5. Loss of MICU1 exacerbates Ca^{2+} overload and result in MM cell stress.
(A) Ca^{2+} levels in MM cells were determined by measuring Rhod-2AM and MitoTracker fluorescence with a confocal laser-scanning microscope **(B)** Fold change of $[Ca^{2+}]_m$ in NC and MICU1-KD MM cells. **(C)** Fold change of $[Ca^{2+}]_m$ in NC and MICU1-KD MM cells after BTZ treatment. **(D)** Flow cytometry analysis to measure the mitochondrial superoxide level in MICU1-KD and NC MM cells using MitoSOX Red staining. Rotenone was used as a positive control. **(E)** Relative mean fluorescence intensity (MFI) of MitoSOX Red fluorescence in MICU1-KD and NC MM cells. **(F)** Frequency of apoptosis cells after BTZ treatment. **(G)** Fold change of $[Ca^{2+}]_m$ in Vec and HRP2-OE cells after BTZ treatment. **(H)**Relative MFI of MitoSOX fluorescence in Vec and HRP2-OE MM cells. Rotenone was used as a positive control. **(I)** Representative confocal images of ROS production in Vec and HRP2-OE MM cells after BTZ treatment. **(J)** Relative ROS levels of Vec and HRP2-OE MM cells after BTZ treatment (n = 6). **(K)** Representative Western blotting ($n = 3$) shows the knockdown effects in MICU1-KD MM cells infected with lentivirus carrying shRNAs targeting two different coding sequencing of HRP2 gene (shRNA1, 2) compared to the NC. **(L)** Fold change of $[Ca^{2+}]_m$ in NC and HRP2-KD MICU1-KD MM cells after BTZ treatment. **(M)**Relative MFI of MitoSOX Red fluorescence in NC and HRP2-KD MICU1-KD MM cells. Rotenone was used as a positive control. **(N)** Representative confocal images of ROS production in NC and HRP2-KD MICU1-KD MM cells after BTZ treatment **(O)** Frequency of apoptosis cells after BTZ treatment. Two-sided P values were determined by Student's t-test. Data are presented as mean ± SD.

sensitivity to BTZ treatment, as evidence by significant reduction of tumor burden (Fig. 6**D**), and alleviated bone lesion causing by MM growth, by measuring the bone volume density (BV/TV), trabecular numbers (Tb. N), trabecular thickness (Tb. Th), and trabecular separation (Tb. Sp) of the metaphyseal regions (Fig. 6**E**-6**G**). These results provide clear evidence that targeting MICU1 in MM may be a viable strategy for overcoming BTZ- resistance of MM cells.

Discussion

Despite extensive researches on chemoresistance into chemoresistance mechanisms associated with PI-based treatments, the fundamental basis is still obscure. In the present study, we disclose an important epigenetic machinery of HRP2 in regulating MICU1 and maintaining mitochondrial Ca^{2+} homeostasis, thereby altering chemosensitivity of MM cells.

While there is accumulating evidence establishing a clear association between epigenetic modification and myeloma progression [31–33], the specific effects and mechanisms of HRP2 in the MM drug resistance remain unclear. Through screening differentially expressed genes in our established BTZ-resistant MM cells, we observed a significant down-regulation of HRP2. Unlike its roles in solid tumor [7], our study demonstrated that HRP2 acts more like a tumor suppressor for MM progression. In this context, we identified a novel role for HRP2 in regulating chemoresistance of MM through modulating MICU1-mediated Ca^{2+} homeostasis in mitochondria. Relevant evidence demonstrates that the Ca^{2+} uniporter-channel complex mediates entry of Ca^{2+} into mitochondria [34]. Silencing of MICU1 causes mitochondrial Ca^{2+} overload [35], we hypothesize that HRP2 may affect mitochondria stress by negatively regulating MICU1 gene expression, thereby inducing apoptosis in MM cells. Increasing evidence has shown a strong correlation between $[Ca^{2+}]_m$ disturbance and mitochondrial stress in the tumor cell apoptosis [36,37]. MICU1 plays a vital role as an essential component of the mitochondrial inner membrane Ca^{2+} channel in preventing mitochondrial Ca^{2+} overload [15]. Our hypothesis was supported by the fact that silencing of MICU1 resulted in $[Ca^{2+}]_m$ uptake and sensitivity to BTZ treatment in MM cells. Meanwhile, increased Ca^{2+}load led to the accumulation of mtROS, resulting in cellular stress. Actually, our previous research on HRP2 has found that suppression of HRP2 expression increases the resistance of MM to bortezomib by negatively regulating endoplasmic reticulum (ER) stress [13]. Since mitochondrial modulation undoubtedly serves as an adaptive strategy for overcoming tumor drug resistance [38], our study thus proposes the translational merit of targeting HRP2 in managing refractory or relapsed

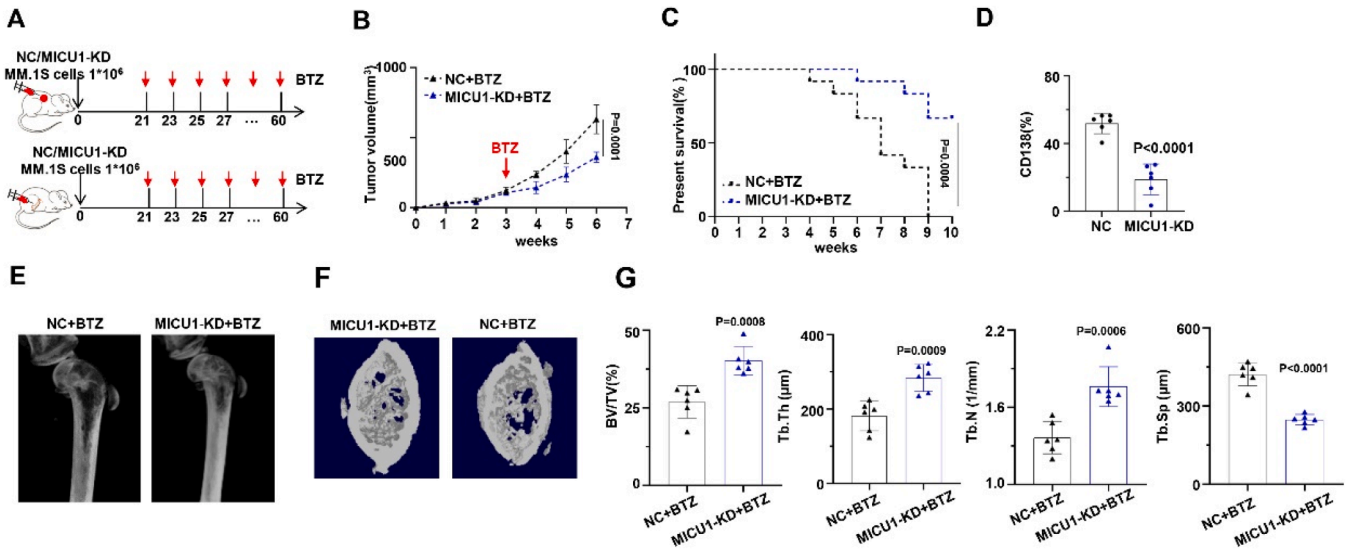

Fig. 6. Targeting MICU1 sensitizes MM cells to BTZ treatment and *in vivo*.
(**A**) Schematic diagram illustrating the BTZ treatment of intra-bone model subcutaneous injection and intra-bone model derived from NSG mice ($n = 6$). **(B)** Growth curve of BTZ-treated bearing tumors in mice, derived from NC and MICU1-KD MM.1S cells ($n = 6$). **(C)** Kaplan-Meier curves showing survival of mice with BTZ-treated bearing tumors derived from NC and MICU1-KD MM.1S cells ($n = 12$). Two-sided *P*-values were analyzed using log-rank test, data are presented as mean ± SD. **(D)** FACS analysis of $CD138^+$ cells in the BM of MM mice after BTZ treatment **(E)** Representative microCT reconstructions of mouse femurs BTZ-treated bearing tumors, derived from NC and MICU1-KD MM.1S cells ($n = 6$). **(F)** 3D reconstructions of bone trabecula in metaphyseal regions ($n = 6$). (**G**) Quantification of microCT analysis of bone volume ratio to tissue volume (BV/TV), trabecular thickness (Tb. Th), and trabecular number (Tb. N) and trabecular separation (Tb.Sp) ($n = 6$). Two-sided *P* values were determined by Student's *t*-test; data are presented as mean ± SD.

MM patients in the clinic.

Importantly, our study substantiates the epigenetic machinery of HRP2 in regulating MICU1 expression both in vitro and in HRP2-knockout mice. HRP2 contains a N-terminal PWWP domain, which preferentially binding to H3K9me3, H3K27me3 and H 3K36me2 [12]. It also interacts DPF3a to recruit SMARCA4/BRG1/BAF190A complex and activates myogenic genes expression by augmenting chromatin accessibility [39], promotes DNA double-strand breaks (DSBs) repair by recruiting the DNA endonuclease RBBP8 [12] and enhances cellular growth [7]. Our previous study has dissected the HRP2-MINA complex in suppressing H3K27me3 modification at the H 3K36me2 abundant TSS regions of target genes, so that promotes expressions of genes governing endoplasmic reticulum (ER) stress [13]. In the current study, we further disclosed that HRP2 suppression resulted in augmentation of H3K27Ac on MICU1 promoter, which is believed a transcriptional activation marker or a super enhancer marker [40]. The alternation of this modification causes enhanced chromatin accessibility and phosphorylation of RNA pol II (Ser5), which is believed a marker of transcription initiation [27]. Thus, the overall significance of this study lies in elucidating the mechanism of the HRP2/MICU1 axis to induce mitochondrial dysfunction and BTZ-resistance of MM cells. However, the limitation of the current study is that we did not clarify how HRP2 rebalances H3K27me3 and H3K27Ac. This may be due to the fact that both modifications share the same site and exhibit antagonistic effects [41], which need to be further investigated.

Conclusion

In summary, our study identifies HRP2 as a critical player in aberrant Ca^{2+} uptake, elucidates the role of MICU1 in MM drug resistance and highlights the significance of regulating MICU1 under high-risk conditions of mitochondrial Ca^{2+} overload. These findings contribute new insights into understanding the development of chemoresistance and present a convincing argument for exploring new strategies to upregulate HRP2 expression to regain sensitivity in RRMM patients.

Declarations

Ethics approval and consent to participate

This study was approved by the Ethics Committee of Tianjin Medical University Cancer Hospital and Research Institute, and all protocols conformed to the Ethical Guidelines of the World Medical Association Declaration of Helsinki. Signed informed consent was obtained from each participating individual prior to participation in the study.

Consent for publication

All authors concur the publication.

Funding

This work was supported by the National Natural Science Foundation of China (82000216 Q Li; 82070221, 82370209, Z.Q. Liu; 82270208, YF Wang) and Tianjin Science and Technology Plan Project (21JCYBJC00290).

Availability of data and materials

The data underlying this article will be shared on reasonable request to the corresponding author. The RNA-seq data can be publicly found at the Gene Expression Omnibus database under accession number GSE267207. The ATAC-seq data can be found under the accession number GSE176547 [13].

CRediT authorship contribution statement

Qian Li: Conceptualization, Validation, Writing – original draft, Funding acquisition. **Ziyi Peng:** Conceptualization, Methodology, Validation, Writing – original draft. **Li Lin:** Methodology, Validation. **Zhiying Zhang:** Methodology, Validation. **Jing Ma:** Data curation, Visualization. **Lin Chen:** Data curation, Visualization. **Su Liu:** Data curation, Visualization. **Shuang Gao:** Data curation, Visualization.

Linchuang Jia: Methodology, Validation. **Jingjing Wang:** Methodology, Validation. **Zeng Cao:** Data curation, Validation. **Xingli Zhao:** Funding acquisition, Writing – review & editing. **Zhiqiang Liu:** Conceptualization, Funding acquisition, Writing – review & editing. **Yafei Wang:** Funding acquisition, Writing – review & editing.

Declaration of competing interest

The authors declare that they have no known competing financial interests or personal relationships that could have appeared to influence the work reported in this paper.

References

[1] S.K. Kumar, V. Rajkumar, R.A. Kyle, M. van Duin, P. Sonneveld, M.V. Mateos, et al., Multiple myeloma, Nat. Rev. Dis. Primers. 3 (2017) 17046.
[2] A.J. Cowan, D.J. Green, M. Kwok, S. Lee, D.G. Coffey, L.A. Holmberg, et al., Diagnosis and management of multiple myeloma: a review, JAMa 327 (2022) 464–477.
[3] H. Brenner, A. Gondos, D. Pulte, Recent major improvement in long-term survival of younger patients with multiple myeloma, Blood 111 (2008) 2521–2526.
[4] J.N. Vo, Y.M. Wu, J. Mishler, S. Hall, R. Mannan, L. Wang, et al., The genetic heterogeneity and drug resistance mechanisms of relapsed refractory multiple myeloma, Nat. Commun. 13 (2022) 3750.
[5] P. Sonneveld, Management of multiple myeloma in the relapsed/refractory patient, Hematology. Am. Soc. Hematol. Educ. Program. 2017 (2017) 508–517.
[6] P. Moreau, S.K. Kumar, J. San Miguel, F. Davies, E. Zamagni, N. Bahlis, et al., Treatment of relapsed and refractory multiple myeloma: recommendations from the International Myeloma Working Group, Lancet Oncol. 22 (2021) e105–e118.
[7] K. Gao, C. Xu, X. Jin, R. Wumaier, J. Ma, J. Peng, et al., HDGF-related protein-2 (HRP-2) acts as an oncogene to promote cell growth in hepatocellular carcinoma, Biochem. Biophys. Res. Commun. 458 (2015) 849–855.
[8] J. Yang, A.D. Everett, Hepatoma-derived growth factor binds DNA through the N-terminal PWWP domain, BMC. Mol. Biol. 8 (2007) 101.
[9] X. Min, J. Wen, L. Zhao, K. Wang, Q. Li, G. Huang, et al., Role of hepatoma-derived growth factor in promoting de novo lipogenesis and tumorigenesis in hepatocellular carcinoma, Mol. Oncol. 12 (2018) 1480–1497.
[10] S. Van Belle, S. El Ashkar, K. Cermakova, F. Matthijssens, S. Goossens, A. Canella, et al., Unlike its paralog LEDGF/p75, HRP-2 is dispensable for MLL-R leukemogenesis but important for leukemic cell survival, Cells 10 (2021).
[11] E. Martinez-Garcia, R. Popovic, D.J. Min, S.M. Sweet, P.M. Thomas, L. Zamdborg, et al., The MMSET histone methyl transferase switches global histone methylation and alters gene expression in t(4;14) multiple myeloma cells, Blood 117 (2011) 211–220.
[12] A. Baude, T.L. Aaes, B. Zhai, N. Al-Nakouzi, H.Z. Oo, M. Daugaard, et al., Hepatoma-derived growth factor-related protein 2 promotes DNA repair by homologous recombination, Nucleic. Acids. Res. 44 (2016) 2214–2226.
[13] J. Wang, X. Zhu, L. Dang, H. Jiang, Y. Xie, X. Li, et al., Epigenomic reprogramming via HRP2-MINA dictates response to proteasome inhibitors in multiple myeloma with t(4;14) translocation, J. Clin. Invest. 132 (2022).
[14] L. Ji, F. Liu, Z. Jing, Q. Huang, Y. Zhao, H. Cao, et al., MICU1 Alleviates diabetic cardiomyopathy through mitochondrial Ca(2+)-dependent antioxidant response, Diabetes 66 (2017) 1586–1600.
[15] K. Mallilankaraman, P. Doonan, C. Cardenas, H.C. Chandramoorthy, M. Muller, R. Miller, et al., MICU1 is an essential gatekeeper for MCU-mediated mitochondrial Ca(2+) uptake that regulates cell survival, Cell 151 (2012) 630–644.
[16] D. Tomar, M. Thomas, J.F. Garbincius, D.W. Kolmetzky, O. Salik, P. Jadiya, et al., MICU1 regulates mitochondrial cristae structure and function independently of the mitochondrial Ca(2+) uniporter channel, Sci. Signal. 16 (2023) eabi8948.
[17] G. Csordas, T. Golenar, E.L. Seifert, K.J. Kamer, Y. Sancak, F. Perocchi, et al., MICU1 controls both the threshold and cooperative activation of the mitochondrial Ca(2)(+) uniporter, Cell Metab. 17 (2013) 976–987.
[18] D. De Stefani, A. Raffaello, E. Teardo, I. Szabo, R. Rizzuto, A forty-kilodalton protein of the inner membrane is the mitochondrial calcium uniporter, Nature 476 (2011) 336–340.
[19] S. Orrenius, B. Zhivotovsky, P. Nicotera, Regulation of cell death: the calcium-apoptosis link, Nat. Rev. Mol. Cell Biol. 4 (2003) 552–565.
[20] P.K. Chakraborty, S.B. Mustafi, X. Xiong, S.K.D. Dwivedi, V. Nesin, S. Saha, et al., MICU1 drives glycolysis and chemoresistance in ovarian cancer, Nat. Commun. 8 (2017) 14634.
[21] Y. Wang, L. Chen, Q. Li, S. Gao, S. Liu, J. Ma, et al., Inositol polyphosphate 4-phosphatase type II is a tumor suppressor in multiple myeloma, Front. Oncol. 11 (2021) 785297.
[22] Z. Peng, J. Wang, J. Guo, X. Li, S. Wang, Y. Xie, et al., All-trans retinoic acid improves NSD2-mediated RARalpha phase separation and efficacy of anti-CD38 CAR T-cell therapy in multiple myeloma, J. ImmunOther Cancer 11 (2023).
[23] Y. Yang, G. Zhang, F. Guo, Q. Li, H. Luo, Y. Shu, et al., Mitochondrial UQCC3 modulates hypoxia adaptation by orchestrating OXPHOS and glycolysis in hepatocellular carcinoma, Cell Rep. 33 (2020) 108340.
[24] X. Li, S. Wang, Y. Xie, H. Jiang, J. Guo, Y. Wang, et al., Deacetylation induced nuclear condensation of HP1gamma promotes multiple myeloma drug resistance, Nat. Commun. 14 (2023) 1290.
[25] Y. Xie, N. Han, F. Li, L. Wang, G. Liu, M. Hu, et al., Melatonin enhances osteoblastogenesis of senescent bone marrow stromal cells through NSD2-mediated chromatin remodelling, Clin. Transl. Med. 12 (2022) e746.
[26] H. Jiang, L. Wang, Q. Zhang, S. Wang, L. Jia, H. Cheng, et al., Bone marrow stromal cells dictate lanosterol biosynthesis and ferroptosis of multiple myeloma, Oncogene (2024).
[27] M. Tellier, J. Zaborowska, L. Caizzi, E. Mohammad, T. Velychko, B. Schwalb, et al., CDK12 globally stimulates RNA polymerase II transcription elongation and carboxyl-terminal domain phosphorylation, Nucleic. Acids. Res. 48 (2020) 7712–7727.
[28] K. Xue, D. Wu, Y. Wang, Y. Zhao, H. Shen, J. Yao, et al., The mitochondrial calcium uniporter engages UCP1 to form a thermoporter that promotes thermogenesis, Cell Metab. 34 (2022) 1325–1341, e1326.
[29] G. Gherardi, H. Monticelli, R. Rizzuto, C. Mammucari, The mitochondrial Ca(2+) uptake and the fine-tuning of aerobic metabolism, Front. Physiol. 11 (2020) 554904.
[30] L. Zhang, Z. Wang, T. Lu, L. Meng, Y. Luo, X. Fu, et al., Mitochondrial Ca(2+) overload leads to Mitochondrial oxidative stress and delayed meiotic resumption in mouse oocytes, Front. Cell Dev. Biol. 8 (2020) 580876.
[31] E. Logie, B. Van Puyvelde, B. Cuypers, A. Schepers, H. Berghmans, J. Verdonck, et al., Ferroptosis induction in multiple myeloma cells triggers DNA methylation and histone modification changes associated with cellular senescence, Int. J. Mol. Sci. 22 (2021).
[32] N.H. Ismail, A. Mussa, N.A. Zakaria, M.J. Al-Khreisat, M.A. Zahidin, N.N. Ramli, et al., The role of epigenetics in the development and progression of Multiple myeloma, Biomedicines. 10 (2022).
[33] M. Alzrigat, A.A. Parraga, H. Jernberg-Wiklund, Epigenetics in multiple myeloma: from mechanisms to therapy, Semin. Cancer Biol. 51 (2018) 101–115.
[34] R. Payne, H. Hoff, A. Roskowski, J.K. Foskett, MICU2 Restricts spatial crosstalk between InsP(3)R and MCU channels by regulating threshold and gain of MICU1-mediated inhibition and activation of MCU, Cell Rep. 21 (2017) 3141–3154.
[35] D. Pendin, E. Greotti, T. Pozzan, The elusive importance of being a mitochondrial Ca(2+) uniporter, Cell Calcium 55 (2014) 139–145.
[36] Y. Luo, J. Ma, W. Lu, The significance of mitochondrial dysfunction in cancer, Int. J. Mol. Sci. 21 (2020).
[37] J.M. Winter, T. Yadav, J. Rutter, Stressed to death: mitochondrial stress responses connect respiration and apoptosis in cancer, Mol. Cell 82 (2022) 3321–3332.
[38] R. Avolio, D.S. Matassa, D. Criscuolo, M. Landriscina, F. Esposito, Modulation of mitochondrial metabolic reprogramming and oxidative stress to overcome chemoresistance in cancer, Biomolecules. 10 (2020).
[39] X. Zhu, B. Lan, X. Yi, C. He, L. Dang, X. Zhou, et al., HRP2-DPF3a-BAF complex coordinates histone modification and chromatin remodeling to regulate myogenic gene transcription, Nucleic. Acids. Res. 48 (2020) 6563–6582.
[40] T.H. Beacon, G.P. Delcuve, C. Lopez, G. Nardocci, I. Kovalchuk, A.J. van Wijnen, et al., The dynamic broad epigenetic (H3K4me3, H3K27ac) domain as a mark of essential genes, Clin. Epigenetics. 13 (2021) 138.
[41] J. Kim, Y. Lee, X. Lu, B. Song, K.W. Fong, Q. Cao, et al., Polycomb- and methylation-independent roles of EZH2 as a transcription activator, Cell Rep. 25 (2018) 2808–2820, e2804.